Fiber feature map based landmark initialization for highly deformable DTI registration

COMP 992 Report by Ravikiran Janardhana[1]

Co-Authors: Aditya Gupta[2,4], Matthew Toews[3], Yogesh Rathi[3], John Gilmore[4], Maria Escolar[2], Martin Styner[1,4]

[1]Dept Computer Science, University of North Carolina, Chapel Hill, [2]Dept Pediatrics, University of Pittsburgh, PA, USA; [3]Harvard Medical School, Boston MA; [4]Dept Psychiatry, University of North Carolina, Chapel Hill.

Abstract. This paper presents a novel pipeline for the registration of diffusion tensor images (DTI) with large pathological variations to normal controls based on the use of a novel feature map derived from white matter (WM) fiber tracts. The research presented aims towards an atlas-based DTI analysis of subjects with considerable brain pathologies such as tumors or hydrocephalus. In this paper, we propose a novel feature map that is robust against variations in WM fiber tract integrity and use these feature maps to determine a landmark correspondence using a 3D point correspondence algorithm. This correspondence drives a deformation field computed using Gaussian radial basis functions (RBF). This field is employed as an initialization to a standard deformable registration method like Demons. We present early preliminary results on the registration of a normal control dataset to a dataset with abnormally enlarged lateral ventricles affected by fatal demyelinating Krabbe disease. The results are analyzed based on a regional tensor matching criterion and a visual assessment of overlap of major WM fiber tracts. While further evaluation and improvements are necessary, the results presented in this paper highlight the potential of our method in handling registration of subjects with severe WM pathology.

Keywords: fiber feature map, 3D point correspondence, DTI, large deformation fields

1 Introduction

Diffusion tensor imaging (DTI) has proven especially of value in clinical studies of white matter (WM) integrity in the developing brain. In this paper, we focus on the application of DTI in a natural history study of a particularly devastating WM demyelinating disease called Krabbe [1]. Previous studies show that neonates with infantile Krabbe disease have lower fractional anisotropy (FA) across the corpus callosum and along the DTI fiber bundle of internal capsules (IC) when compared with healthy age-matched controls [2]. Based on the above findings, atlas-based fiber tract analysis is used for analyzing DTI of Krabbe

subjects [3]. For accurate analysis of WM fiber tracts it is crucial to establish a registration-based voxel-wise correspondence between a normal control and the Krabbe subjects.

In addition to the pathological WM integrity, untreated infantile Krabbe cases may develop significantly enlarged lateral ventricles, a condition similar to hydrocephalus. The enlargement of the lateral ventricles push the fiber tracts against the skull, making it very difficult to analyze these images with an atlas-based methodology. In our studies, the clinicians are interested to investigate fiber-tracts-based DTI analysis in such natural history cases as this reveals crucial information about disease progression.

The research in this paper is a step towards the analysis of these fiber tracts. The paper presents a method to determine point correspondences between the subject case and the normal control automatically by computing novel feature maps from the DWI data. These feature maps highlight the crossing fiber regions and are based on voxel-wise fiber density and entropy computations. The point correspondences are used to determine a deformation field via Gaussian radial basis functions (RBF) [4]. This deformation field is then used to initialize a standard registration method. The results are presented on a Krabbe subject with particularly abnormal enlarged ventricles to highlight the potential of the proposed approach.

The main contributions of this paper include a novel feature map determined from DWI data, which highlights the single and crossing fiber geometry, while being robust against variations in WM fiber tract integrity, a feature desirable in many WM demyelinating pathologies. Also this paper proposes a novel registration pipeline, which uses this feature map alongside a 3D correspondence algorithm and a Gaussian RBF to initialize standard registration algorithms to handle high anatomical deformations.

2   Methodological Background

Registration of DTIs is particularly challenging, as DTI data is multi-dimensional and the tensor orientations after image transformations must remain consistent with the anatomy. Prior to the development of full-tensor-based registration methods, DTI registration was performed with traditional image registration algorithms on scalar images derived from the DTI. The performance of scalar and full tensor registration algorithms are compared for Krabbe neonates [5] and the full-tensor-based DTI-TK [6] method showed the most accurate performance.

The major drawback when using DTI derived FA scalar map in the registration of WM demyelinating pathologies is that the FA values are highly affected by the pathology. While intensity normalization approaches have been employed to reduce the impact of this issue, major pathologies cannot be handled in this way. This drives the motivation of our proposed work towards a feature map that is robust against variations in WM fiber tract integrity. Several authors have used other DTI derived scalar maps such as radial diffusivity (RD), mean diffusivity (MD) or even multichannel registration [7] with several of these feature maps.

But again these methods rely on properties derived from the fiber tracts, which may be an issue in pathologies such as Krabbe with large structural variations. The motivation of our proposed feature map is to highlight voxel-wise fiber geometry features such as crossing fiber and single fiber situations, which can be largely independent of the fiber tract properties and thus be used as the driving force for registration. The next section discusses the methodology behind generating these feature maps, the point correspondence, initial deformation field and the final deformation.

3 Method

The first part of this section describes the steps involved in generating the novel feature map from DWI data. The second part describes the algorithm for determining the point correspondence on these feature maps. This is followed by a description on using the point correspondences to determine an initial deformation field through Gaussian RBF. Finally the steps involved in using this deformation field as an initialization to a standard registration algorithm are discussed.

3.1 Feature Map Generation

In this section, we present the steps involved in generating the feature map from the raw diffusion weighted image (DWI) and the image mask. First, we perform a 2-tensor unscented-Kalman-filter-based tractography [8] in order to obtain the fiber tracts image. Once the fiber tracts have been generated, we compute two main features, namely number of fiber segments per voxel and entropy of fiber orientations per voxel. We normalize and combine these two features in order to develop the feature image. The following sections describe each step of the feature map generation in detail.

Fiber Tracts Generation The fiber tracts are generated from the raw DWI image and the image mask by performing a 2-tensor unscented-Kalman-filter-based (ukf) tractography. Unlike many of the existing techniques, in ukf-based tractography, fiber tracking is formulated as causal estimation: at each step of tracing the fiber, the current estimate of the signal is guided by the previous. To do this, the signal is modeled as a discrete mixture of Watson directional functions and tractography is performed within a filtering framework. Starting from a seed point, each fiber is traced to its termination using an unscented Kalman filter to simultaneously fit the signal and propagate in the most consistent direction. Despite the presence of noise and uncertainty, this provides an accurate estimate of the local structure at each point along the fiber. The in-depth details of the tractography can be found in [8].

While generating the fiber tracts, we can configure various parameters, the most important ones being number of seeds per voxel, seed FA limit and minimum FA to continue tractography. Figure 1 shows the fiber tracts generated for

different parameter configurations. Based on visual assessment of the fiber tracts generated, for our experiments, we configured the number of seeds per voxel as 8, the seed FA limit as 0.18 and the minimum FA to continue tractography as 0.12. The minFA and seedFA are set very low as the FA values are very low in Krabbe cases.
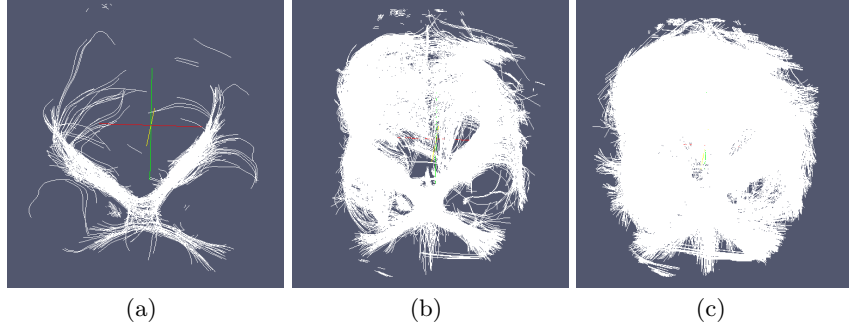

(a)   (b)   (c)

Fig. 1. The figures show the fiber tracts generated at different parameter configurations. (a) seedFA = 0.30, minFA = 0.25, seedsPerVoxel = 1, (b) seedFA = 0.20, minFA = 0.20, seedsPerVoxel = 4, (c) seedFA = 0.18, minFA = 0.12, seedsPerVoxel = 8.

Fiber Segments per voxel In this step, we traverse through all the fiber segments in the fiber tracts generated; we identify which voxel a particular fiber segment belongs to and increment its counter by one. The result of this step is an image where the value at a particular voxel indicates the number of fiber segments it contains and thus indicates the density of fibers at that voxel.

Entropy of Fiber Orientations In order to compute the entropy of fiber orientations at a particular voxel, we first need to define what is the fiber orientation at a voxel. Consider the below example in Figure 2, where a single fiber passes through the fiber points p1, p2 and p3 within a particular voxel. The fiber orientation at a fiber point is defined as the direction of the tangent joining its neighboring fiber segment points. At the boundary fiber points, the fiber orientation is defined as the direction of the line connecting it to the previous or subsequent fiber point. The fiber orientation at a voxel can now be defined as a tuple of fiber orientations at the fiber points contained in the voxel.

The next step is to compute the histogram (see Figure 2) of these fiber orientations at each voxel. This histogram computed is on a unit sphere that is subdivided into equal regions by fitting a platonic solid such as an icosahedron onto the surface of the sphere with a sub-division level of 6. At the subdivision level of 6, we get 492 icosahedron vertices. Given a fiber orientation, we approximate it to a particular icosahedron triangular face and add it to the icosahedron
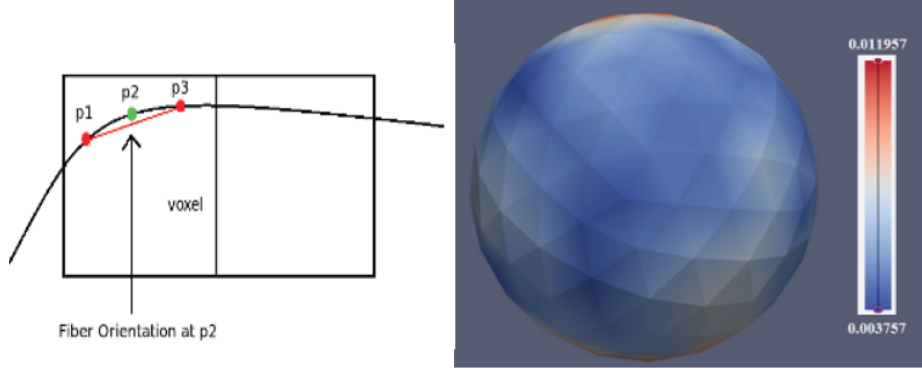
Fig. 2. Fiber orientation computed at a fiber segment point and the histogram representing the fiber orientations of a particular voxel on a unit sphere.

vertices using barycentric coordinate system in which the location of the fiber direction is specified as the center of mass, or barycenter, of masses placed at the vertices of a simplex i.e., a triangle in our case.

This histogram is then used to generate the entropy of fiber orientations. Entropy is a measure of disorder, or more precisely unpredictability. For example, a series of coin tosses with a fair coin has maximum entropy, since there is no way to predict what will come next. A string of coin tosses with a coin with two heads and no tails has zero entropy, since the coin will always come up heads. Similarly if there is just a single track fiber, there is less unpredictability and hence lower entropy and if there are multiple fiber tracts and multiple fiber orientations, this means that there is more unpredictability and hence higher entropy.

Using the histogram, we compute entropy of fiber orientations per voxel as below:

$$H(X) = -\sum_{i=1}^{n} p(x_i) \log_b p(x_i) \qquad (1)$$

where, $H(X)$ is the entropy of fiber orientation at a particular voxel, $p(x_i)$ is the probability of a fiber orientation to be x_i and n represents all possible fiber orientations.

Combining Features to Obtain Feature Map In order to obtain the feature map, we first normalize the two features, namely fiber segments per voxel and entropy of fiber orientations per voxel by dividing each of these by their respective maximum over the entire image. The feature map is then obtained by computing the square root of the product of normalized values of the two features. The reasoning behind this formulation is explained in the following paragraphs.

$$F_i(X) = \sqrt{\frac{H_i(X)}{H_{max}(X)} * \frac{fs_i(X)}{fs_{max}(X)}} \qquad (2)$$

where $F_i(X)$, $H_i(X)$ and $fs_i(X)$ are the feature map value, entropy of fiber orientations and the number of fiber segments at voxel i respectively, $H_{max}(X)$ and $fs_{max}(X)$ are the maximum values of entropy of fiber orientations and number of fiber segments over the entire image.

The above formulation is designed to highlight crossing fiber landmarks (see Figure 3) invariant of pathology so that they can be used in the registration process. Equation 2 highlights landmarks and the reasoning as to why it does is explained as follows. If one examines the fiber segments per voxel image, it is bound to have higher intensities in those regions where there are large number of single fiber tracts and multiple fiber tracts. It has lower intensities in regions of fewer or no fiber tracts. The entropy of fiber orientations image has higher intensities in regions of dispersed single fiber tracts and crossing fiber tracts (due to greater variation in fiber orientations). It has lower intensities in uni-directional single fiber tracts or no fiber tracts regions. Hence, by combining these two, we annul the uni-directional single fiber tracts and no fiber tracts regions, thus highlighting the crossing fiber regions or landmarks.
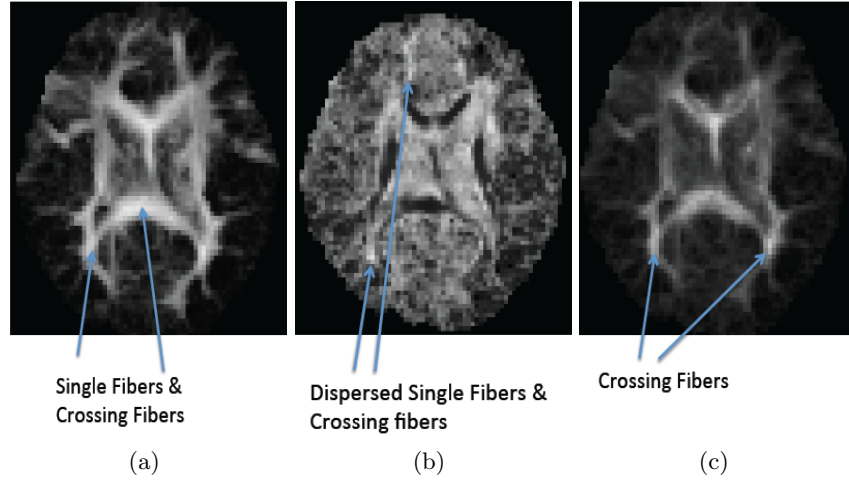

Fig. 3. Feature maps in normal control subject. (a) Fiber Segments per voxel image; (b) Entropy of fiber orientations per voxel image; (c) Combined feature map image. The regions with crossing fibers are marked with arrows and display a high intensity in the final feature map.

3.2   Landmarks with correspondence on feature maps

Deformable intensity-based image registration methods employ local optimization methods that are largely driven by distinctive image structure, i.e., corners or landmarks, and must be correctly initialized in order to ensure convergence to correct solutions. Here, we achieve initialization from a set of robust image-to-image correspondences obtained via a 3D version of the scale-invariant feature transform (SIFT) matching technique of Lowe et al [9]. The first stage of this technique is scale-space extrema detection. This stage of computation identifies locations that are invariant to scale change of the image by searching for stable features across all possible scales, using a continuous function of scale known as scale space. The scale space of an image is defined as the function, $L(x, y, z, \sigma)$, that is produced from the convolution of a variable-scale Gaussian, $G(x, y, z, \sigma)$, with an input image, $I(x, y, z)$ as below:

$$L(x, y, z, \sigma) = G(x, y, z, \sigma) * I(x, y, z), \tag{3}$$

In order to efficiently detect stable keypoint locations in space, Lowe et al [9] propose a difference-of-Gaussian function convolved with the image, $D(x, y, z, \sigma)$, which can be computed from the difference of two nearby scales separated by a constant multiplicative factor k:

$$D(x, y, z, \sigma) = (G(x, y, z, k\sigma) - G(x, y, z, \sigma)) * I(x, y, z) \tag{4}$$
$$= L(x, y, z, k\sigma) - L(x, y, z, \sigma)$$

where $G(x, y, z, \sigma)$ represents the convolution with a Gaussian operator of variance σ^2 and k is a constant. In order to detect local maxima and minima of $D(x, y, z, \sigma)$, each sample point is compared to its eight neighbors in the current image and nine neighbors in the scale above and below. It is selected only if it is larger than all of these neighbors or smaller than all of them. Once a keypoint candidate has been found by comparing a pixel to its neighbors, the next step is to perform a detailed fit to the nearby data for location, scale, and ratio of principal curvatures. This information allows points to be rejected that have low contrast (and are therefore sensitive to noise) or are poorly localized along an edge. Each keypoint is also assigned a consistent orientation [9] based on local image properties, as a result, the keypoint descriptor can be represented relative to this orientation and therefore achieve invariance to image rotation.

Thus, each keypoint is now assigned an image location, scale and orientation. These parameters impose a repeatable local 3D coordinate system in which to describe a local image region, and therefore provide invariance to these parameters. The next step computes a descriptor for the local image region that is highly distinctive yet is as invariant as possible to remaining variations. Lowe et al [9] use the local image descriptor computation described by Edelman et al [10] and the details of it are omitted in this report for brevity. Further, image-to-image matching proceeds by computing nearest neighbors between features (location, scale, orientation etc) extracted in different images, based on the Euclidean distances of local image descriptors. Note that due to spatial feature
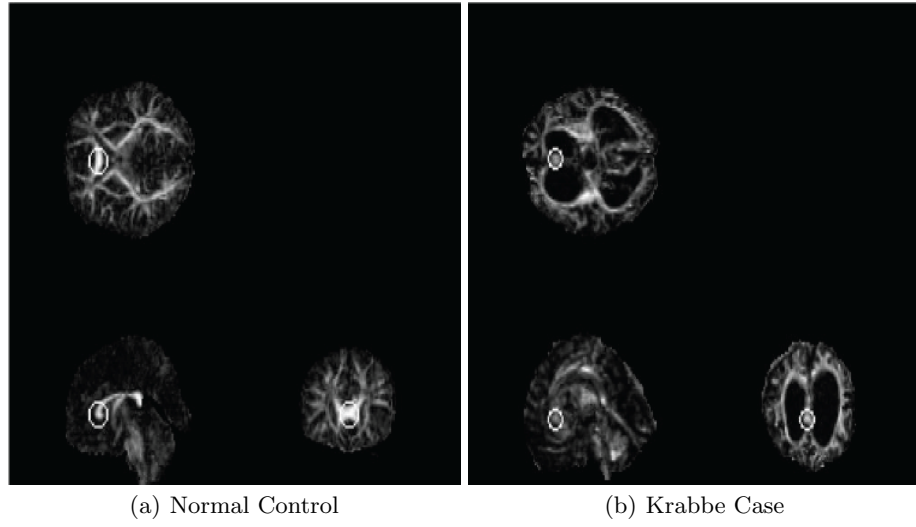
(a) Normal Control   (b) Krabbe Case

Fig. 4. Example of one set of correspondence points.

(a) Moving Image - Normal Control   (b) Result of Demons   (c) Result of DTITK

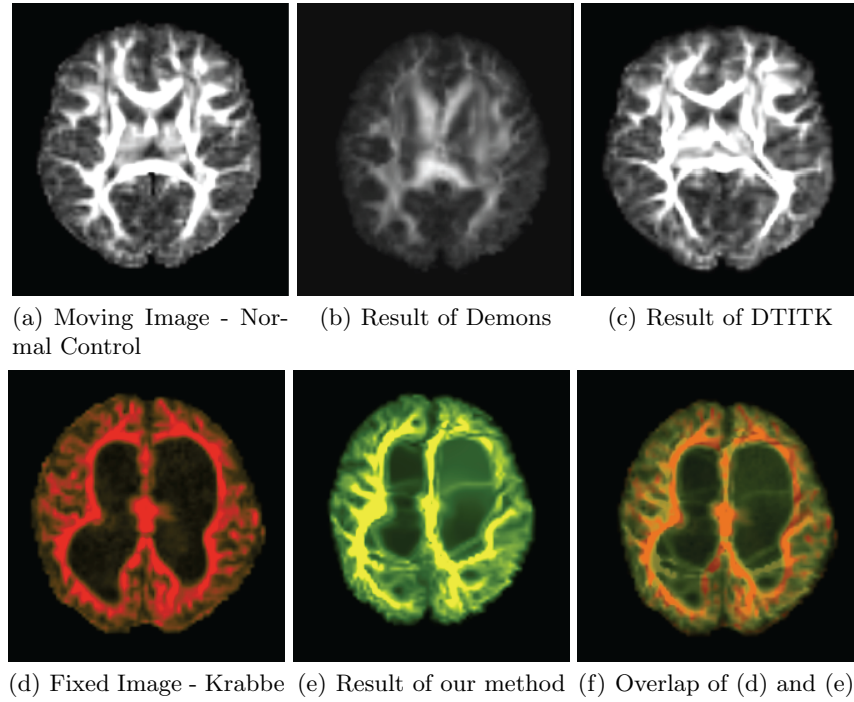(d) Fixed Image - Krabbe (e) Result of our method (f) Overlap of (d) and (e)

Fig. 5. The figure shows the normal control FA map, the Krabbe subject FA map with the registration result with Demons, DTITK and our proposed method.

normalization, nearest neighbors can be computed despite arbitrary global similarity image transforms (i.e. translation, rotation and isotropic scaling). Finally, the Hough transform is applied to determine a set of correspondences that are inliers of a robust image-to-image similarity transform.

3.3 Registration

Due to the large variation between the normal control and the subject with enlarged ventricles, a large deformation field is needed to register these images. Registration failed with the standard registration algorithms, including B-spline-based (fnirt in FSL package), fluid-based (fWarp in FSL), Demons (BRAINSDemonWarp in BRAINS) and also full tensor registration method DTITK within the DTI-Toolkit package. All the above methods failed to provide the large deformation required to register these images, particularly in the regions around the enlarged ventricles (figure 4).

To determine the large local deformation field, we first compute the landmark correspondences described in Section 3.2. These landmarks are then used in a landmark-based image registration method provided by the plastimatch toolkit [11]. The landmark-based registration internally uses non-truncated Gaussian radial basis function (RBF) to make local registrations and generates a deformation field by solving a system of linear equations which is computationally very efficient as compared with algorithms based on complex multidimensional minimization. Also, an independent regularization parameter is defined to control the balance between the fidelity of the alignment of landmark pairs and smoothness of the deformation field. The computed landmarks are in general well distributed over the image and hence have the capability to estimate a global deformation field from these local landmarks. A Gaussian RBF decreases with growing distance from the landmark and the RBF asymptotically approaches zero. This property gives the desired advantage of decreasing global influence with higher distance from the landmarks. While we selected a straightforward landmark-based deformation field generation in this work, there is a lot of ongoing research in generating deformation fields from landmark points that potentially can improve the performance of our proposed registration approach. Once the deformation field is obtained, this field is used to initialize an automatic deformable registration method like diffeomorphic Demons registration on intensity normalized FA images. The results of the combined fields, namely the point landmark deformation field and the Demons deformation field on the FA images are presented in the next section.

4 RESULTS

Using the DWI volumes for the subject and the normal control, we generate the feature maps, as described in Section 3.1. Figure 3 shows the image representing the fiber segments per voxel, the normalized entropy and the combined final map. For the image representing the fiber segments per voxel, high intensity

regions are expected and observed in regions of single fiber tracts and crossing fibers, as both capture a large proportion of fiber segments. For the entropy image, the high intensities are regions of dispersed fiber tracts (e.g., close to gray matter) and crossing fiber tracts (due to greater variation in fiber orientations) and lower intensities in unidirectional single fiber tracts (or in regions with lack of fiber tracts). The combination of these two features results in comparatively lower intensities the unidirectional single fiber situation as compared to crossing fiber situations. Furthermore, locations close or in gray matter display very low intensities in the combined map. In comparison, FA maps cannot successfully highlight crossing fiber locations as these have often similar intensities as WM regions close to gray with largely dispersed fibers.

The combined feature map images for the subject and the normal control are then used as input to determine the point landmark correspondence. The point correspondences are used as inputs to the Gaussian RBF to determine the initial deformation field. This deformation field is used to initialize the Demons algorithm applied on the subject and the normal control FA images. Figure 5 shows the FA images of the Krabbe case and the normal control and shows the results of Demons, DTITK and our proposed method. Clearly, Demons and DTITK fail to produce the required deformation to push the corticospinal and the internal capsule tracts towards the necessary locations in the pathological subject. Also, the figure shows the overlap of the target and image registered with our method to show the performance of our method. The regions in orange indicate the WM fiber tracts that are aligned successfully. From this overlap figure, a considerable success in registration is obtained for the major tracts - the genu, splenium and the internal capsule tracts.
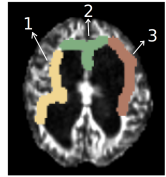
To evaluate the registration, we use average regional matching criterion that is tailored to atlas-based analysis methods. The orientation agreement between the principal eigenvectors of the source e_{source} and the target e_{target} weighted with the FA value of the target of each voxel of a particular region is the basis of this criterion. Regions of interest (ROI) on the Krabbe subject are defined representing major fiber tracts. For a ROI r, the average regional matching criterion is defined as:

$$RegMatch_r = \frac{1}{N_r} \sum_{i=1}^{N_r} |e_{source}.e_{target}|.FA_{target}.N_r \qquad (5)$$

representing number of voxels in region r. The RegMatch percent values for the comparison of Demons, DTITK and our proposed method for three ROIs (100% indicates perfect registration) are shown in Figure 6. Considering the three ROIs, our proposed shows an improvement of 15.4% over DTITK and 22.8% over Demons method.

5 DISCUSSIONS and CONCLUSIONS

In this paper, we have presented a novel, fully automatic pipeline to register images with large deformations, particularly subjects that are affected by WM

Label	Voxels Count	Demons	DTITK	Our Method
1	14288	48.057	49.344	73.351
2	13784	50.301	63.763	68.759
3	13448	46.020	53.519	70.784

Fig. 6. Labels on Krabbe case and percentage registration accuracy.

demyelinating pathologies. The novel feature map computed is robust against variations in WM fiber tract integrity and hence yields a good starting point to compute corresponding landmark points. The work presented here shows the potential of our pipeline to register highly deformed images as illustrated on a single, highly pathological case. We have applied the method to several more Krabbe cases with moderate to severely enlarged ventricles with similar success. Nevertheless, the presented registration pipeline is preliminary and several issues still need to be addressed, such as improving the stability of the landmark-based deformation field computation against outliers/bad correspondences. For that purpose, we are currently working on incorporating weights for each landmark-based on their correspondence quality score.

References

1. Escolar, M., Poe, M., Smith, J., Gilmore, J., Kurtzberg, J., Lin, W., Styner, M.: Diffusion tensor imaging detects abnormalities in the corticospinal tracts of neonates with infantile krabbe disease. American Journal of Neuroradiology **30**(5) (May 2009) 1017–1021
2. Guo, A.C., Petrella, J.R., Kurtzberg, J., Provenzale, J.M.: Evaluation of white matter anisotropy in krabbe disease with diffusion tensor mr imaging: Initial experience1. Radiology **218**(3) (2001) 809–815
3. Goodlett, C., Davis, B., Jean, R., Gilmore, J., Gerig, G.: Improved correspondence for dti population studies via unbiased atlas building. **9**(Pt 2) (10 2006) 260–7
4. Fornefett, M., Rohr, K., Stiehl, H.S.: Elastic registration of medical images using radial basis functions with compact support. Proc. Computer Vison and Pattern Recognition (1999) 402407
5. Wang, Y., Gupta, A., Liu, Z., Zhang, H., Escolar, M.L., Gilmore, J.H., Gouttard, S., Fillard, P., Maltbie, E., Gerig, G., Styner, M.: Dti registration in atlas based fiber analysis of infantile krabbe disease. NeuroImage **55**(4) (2011) 1577 – 1586
6. Zhang, H., Yushkevich, P.A., Alexander, D.C., Gee, J.C.: Deformable registration of diffusion tensor mr images with explicit orientation optimization. Medical Image Analysis **10**(5) (2006) 764 – 785
7. Alexander, D.C., Gee, J.C., Bajcsy, R.: Similarity measures for matching diffusion tensor images. British Machine Vision Conference (1999)
8. Malcolm, J.G., Michailovich, O., Bouix, S., Westin, C.F., Shenton, M.E., Rathi, Y.: A ltered approach to neural tractography using the watson directional function. Medical Image Analysis (2010) 58–69

9. Lowe, D.G.: Distinctive image features from scale-invariant keypoints. IJCV **60**(2) (2004) 91–110
10. Edelman, S., Intrator, N., Poggio, T.: Complex cells and object recognition. (1997)
11. Sharp, G., Li, R., Wolfgang, J., Chen, G., Peroni, M., Spadea, M., Mori, S., Zhang, J., Shackleford, J., Kandasamy, N.: Plastimatch-an open source software suite for radiotherapy image processing. Proceedings of the XVIth International Conference on the use of Computers in Radiotherapy (ICCR), Amsterdam, Netherlands (2010)